Universiteit
Leiden
The Netherlands

Blood flow dynamics in the total cavopulmonary connection long-term after Fontan completion

Rijnberg, F.M.

Citation
Rijnberg, F. M. (2023, December 20). *Blood flow dynamics in the total cavopulmonary connection long-term after Fontan completion*. Retrieved from https://hdl.handle.net/1887/3674148

Version:	Publisher's Version
License:	Licence agreement concerning inclusion of doctoral thesis in the Institutional Repository of the University of Leiden
Downloaded from:	https://hdl.handle.net/1887/3674148

Note: To cite this publication please use the final published version (if applicable).

CHAPTER 11

11

Hemodynamic performance of 16-20mm extracardiac conduits in adolescent Fontan patients

Friso M. Rijnberg, Luca van 't Hul, Mark G. Hazekamp, Pieter J. van den Boogaard, Joe F. Juffermans, Hildo J. Lamb, Covadonga Terol Espinosa de Los Monteros, Lucia J.M. Kroft, Sasa Kenjeres, Saskia le Cessie, Monique R.M. Jongbloed, Jos J.M. Westenberg, Arno A.W. Roest, Jolanda J. Wentzel

European Journal of CardioThoracic Surgery 2022

Abstract

Objective

The synthetic extracardiac conduit used for the completion of the Fontan operation in single ventricle patients lacks growth potential and adequacy of 16-20mm conduits for adult Fontan patients remains unknown. This study aims to determine total cavopulmonary connection (TCPC) hemodynamics using computational fluid dynamics (CFD) in adolescent Fontan patients at rest and during simulated exercise and to assess the relationship between conduit size and hemodynamics.

Methods

Patient-specific MRI-based CFD models of the TCPC were performed in 51 extracardiac Fontan patients (median age 16.2 years, Q1-Q3 14.0-18.2) with 16-20mm conduits. Power loss, pressure gradient and normalized resistance were quantified in rest and during simulated exercise, separated into inspiration and expiration. The cross-sectional area (CSA, mean and minimal) of the TCPC vessels were determined and normalized for vessel-specific flow rate (mm^2/L/min). Peak (predicted) VO2 was assessed.

Results

The normalized conduit CSA_{mean} was a median of 35-73% smaller compared to other TCPC vessels (all $P<0.001$). All CFD hemodynamics significantly increased from rest to simulated exercise (all $p<0.001$) and were higher during inspiration compared to expiration ($p<0.001$). A moderate-strong inverse non-linear relationship was present between normalized conduit CSA_{mean} and CFD hemodynamics in rest and exercise. Pressure gradients of ≥1.0 at rest and ≥3.0mmHg during simulated exercise were observed in patients with a conduit ≤45mm^2/L/min. Normalized TCPC resistance weakly correlated with (predicted) peak VO2.

Conclusions

Extracardiac conduits of 16-20mm have become relatively undersized in adolescent Fontan patients, with most adverse hemodynamics observed in patients with a conduit ≤45mm^2/L/min and favorable hemodynamics in patients with a conduit size ≥125mm^2/L/min.

Introduction

Efficient flow is important in cardiology, and especially the Fontan circulation is dependent on optimal flow characteristics. The Fontan procedure or total cavopulmonary connection (TCPC) is the palliative treatment for children with a univentricular heart defect, by connecting the systemic venous return directly with the pulmonary arteries (PAs). Most centers nowadays use an extracardiac Goretex conduit of 16-20mm to connect the inferior vena cava with the PA at the age of 2-4 years old.(1) However, the synthetic extracardiac conduit lacks growth potential and it is currently unknown if 16,18 and 20mm conduits remain adequately sized for adult Fontan patients.

The Fontan circulation is characterized by chronically elevated central venous pressure (CVP) and reduced preload and thereby cardiac output.(2) Efficient TCPC blood flow is important to keep the elevation in CVP and reduction in preload to a minimum.(3,4) Small conduits are an important factor of increased TCPC resistance and should be avoided.(5) Chronic venous hypertension and reduction in preload lead to important morbidity, including liver fibrosis and reduced exercise capacity.(1)

Recently, important blood flow accelerations were observed from the subhepatic inferior vena cava (IVC) towards the conduit 13 years after Fontan completion, indicating that 16 to 20mm conduits had become relatively undersized for adolescent Fontan patients.(6) However, the hemodynamic consequences of undersized conduits in terms of pressure gradients and TCPC resistance at rest and during simulated exercise were not determined. Comprehensive assessment of the state of the Fontan circulation, one of the current gaps in knowledge of the Fontan physiology, is important for evaluation of the current surgical practice of Fontan completion and to optimize management of the expanding group of grown-up Fontan patients.(1) Therefore, the aim of this study is to determine TCPC hemodynamics using computational fluid dynamics (CFD) in a cohort of teenage and adolescent Fontan patients with 16 to 20mm conduits at rest and during simulated exercise and to assess the relationship between conduit size and TCPC hemodynamics.

Methods

Study population

Fontan patients with an extracardiac Goretex conduit prospectively underwent magnetic resonance imaging (MRI) examination between 2018-2021 at the Leiden University Medical Center, Leiden, the Netherlands. All patients >8 years old without

contraindications for MRI were eligible for inclusion. The study was approved by the medical ethical review committee of the hospital (P18.024). Written informed consent was obtained from all patients and/or their parents.

Cardiopulmonary exercise testing

Cardiopulmonary exercise testing (CPET) was performed using a continuous incremental bicycle protocol. Peak VO2 (ml/kg/min) and predicted peak VO2 (%) were determined in all patients with a respiratory exchange ratio >1.0.

Magnetic resonance imaging

Anatomical and two-dimensional (2D) real-time flow MRI acquisition details are presented in Supplemental Table 1. Real-time 2D flow MRI measurements were obtained at the subhepatic inferior vena cava (IVC, below entry of the hepatic veins, HVs), at the extracardiac conduit and at the superior vena cava (SVC). HV flow was determined indirectly by subtracting IVC flow from conduit flow. Flow measurements consisted of 250 real-time (non electrocardiogram-gated) flow acquisitions with continuously monitoring of the respiratory signal using an air-filled abdominal belt. The respiratory signal was used to divide the flow signal into inspiration and expiration phases as previously described.(6)

A three-dimensional (3D) model of the TCPC was created based on lumen segmentation on respiratory-navigator gated sagittal and transversal 2D anatomical stacks. The 3D model included the area between the subhepatic IVC, HVs, SVC and RPA (including the right upper lobe branches) and LPA up to the level of the segmental branches (ITK-SNAP(7)). The TCPC model was smoothed, centerlines were derived and vessel extensions were added at all inlets and outlets.(8)

Geometry analysis

The TCPC was automatically divided into standardized segments (conduit, SVC, RPA (distal to right upper lobe branch) and LPA) as previously described.(9) The mean and minimum CSA of these segments were determined perpendicular to the centerline at 1mm intervals. The CSA of the inlet extensions were reported for the subhepatic IVC and HVs since the contribution of these vessels to the TCPC volume was minimal. The CSA was normalized for the vessel-specific average flow rate (mm^2/L/min) as a marker of functional vessel CSA. Ideally, an optimally sized conduit in Fontan patients results in minimal energy loss and minimal flow stasis. Both of these factors are dependent on the ratio between conduit CSA and the amount of conduit flow which are captured in the normalized conduit CSA_{mean} parameter.

In addition, the change in measured conduit CSA_{mean} versus theoretical implanted conduit CSA_{mean} was reported (16mm=201mm^2, 18mm=254mm^2 and 20mm=314mm^2).

Computational Fluid Dynamics

The 3D TCPC model was meshed with 30 polyhedral elements across the average vessel diameter (0.35-0.45mm elements) with four prism layers at the wall in order to achieve mesh-independent results (ANSYS ICEM v17.1, Inc., Canonsburg, PA). All CFD simulations were performed using commercially available Fluent software (v17.1, ANSYS, Inc., Canonsburg, PA). Respiratory cycle-resolved flowrates were prescribed at the inlets using a parabolic velocity profile. Total HV flow was divided over the individual HVs based on the ratio of their respective CSAs. Constant outflow ratios at the PAs were imposed as the outlet boundary condition and subdivided over side branches based on their respective CSAs.(10) The outflow ratio was determined from ECG-gated 2D flow MRI measurements since 2D real-time flow measurements were not performed in the PAs. A rigid vessel wall was assumed and a no-slip condition prescribed. Blood flow was assumed to be laminar. A Carreau model was used to account for the non-Newtonian blood properties in the TCPC.(11)

Exercise condition

To simulate the effect of increased flow during exercise, resting flow rates were adapted according to a study by Wei et al, in which 2D real-time flow MRI measurements were obtained during supine lower-leg exercise.(12) The total duration of the respiratory cycle was decreased with a factor of 1.6, the inspiratory fraction (inspiratory time vs total respiration time) was increased with a factor of 1.17(13) and time-resolved flow rates were increased by a factor of 2.44 (both subhepatic IVC and HVs) and 1.67 (SVC). The resting PA outflow ratios were assumed to remain the same during exercise.(14)

Hemodynamic parameters

Energetics

All parameters were reported during inspiration, expiration and during the entire respiratory cycle. Power loss (PL, in milliwatt, mW) was determined using the viscous dissipation rate method (15). Power loss based pressure gradient (mmHg) from the inlets towards the outlets was determined as follows(10):

$$\Delta P_{TCPC} = \frac{PL}{Q_s},$$

where PL and Q_s are the total power loss and the total systemic venous return in the corresponding respiratory phase.

The resistance normalized for body surface area (BSA) (in mmHg/L/min/m^2) was determined as follows(10):

Normalized resistance = $\frac{\Delta P_{TCPC}}{\frac{Q_S}{BSA}}$.

Flow stagnation volume

Flow stagnation volume (volume of cells with a velocity <0.01 m/s(16)) was determined in a subset of 15 patients as a marker of thrombosis risk; 5 patients per implanted conduit size (16, 18 and 20mm) matched on average conduit flow rate (range 2.2-4.6 L/min, Supplemental Figure 1). The minimal (at peak flow during inspiration) and maximal flow stagnation volume (at lowest flow during expiration) was determined in the entire TCPC and in the conduit only by manually isolating the conduit from the TCPC (Paraview.org). The minimal flow stagnation is of particular clinical interest, as this is the volume of blood in the TCPC that remains stagnated during the entire respiratory cycle. The volume of cells with a velocity magnitude of 0.00 m/s was excluded from the flow stagnation volume to not take the mesh cells with zero velocity at the vessel wall (no slip condition) into account.

Statistical analysis

Data were presented as median (Q1-Q3) or mean (standard deviation). Correlation analysis was performed using Pearson (r) or Spearman (ρ) correlation (weak 0.3-0.5, moderate 0.5-0.7, strong ≥0.7-0.9 and very strong >0.9). Comparison of parameters between respiratory phases were performed using the Friedman test (adjusted for multiple comparisons using Bonferroni). The non-linear relationship between CFD derived energetics and normalized conduit CSA was analyzed using linear regression after log transformation of both the dependent and independent parameters (power curve). A p-value <0.05 was considered statistically significant. Data were analyzed with SPSS 25.0 (IBM Corp., Armonk, NY, USA) and Graphpad Prism 8.0 (GraphPad Software, La Jolla, California, USA).

Results

Sixty-five sequential patients underwent MRI examination during the study period. Fourteen/65 patients were excluded because of incomplete 2D real-time MRI flow data (n=7), central device related artefacts (n=3) or patients with a lateral tunnel Fontan connection (n=4), resulting in 51 patients that were included in this study. Patient characteristics are reported in Table 1. All patients were recruited from the outpatient clinic and were in relatively good clinical condition (NYHA class I-II). CPET was performed

in 46/51 patients, with 40 patients reaching maximal effort (median time between CPET and MRI 0 days (Q1-Q3 -6-0 days).

Table 1. Patient characteristics

Male/Female, n	24/27
Primary diagnosis, n (%)	
- TA	12 (24)
- HLHS	9 (17)
- DILV + TGA	10 (20)
- DORV	6 (11)
- uAVSD	3 (6)
- ccTGA	4 (8)
- PA + IVS	2 (4)
- Other	5 (10)
Dominant ventricle	
Left, n (%)	30 (59)
Right, n (%)	16 (31)
Biventricular/indeterminate, n (%)	5 (10)
Characteristics at Fontan procedure	
Age at Fontan, years	3.3 (2.7-3.9)
Height, cm	98 (92-102)
Weight, kg	14 (13-16)
BSA, m2	0.63 (0.58-0.67)
Implanted conduit size (16/18/20mm), n	27/18/6
Fenestration, n(%)	31 (61)
Characteristics at time of MRI	
Age at MRI, years	16.2 (14.0-18.2)
Height, cm	168 (163-175)
Weight, kg	59 (50-66)
BSA, m2	1.66 (1.52-1.76)
Time between Fontan and MRI, years	13.1 (10.4-15.8)
NYHA-class I-II, n (%)	51 (100)
Cardiopulmonary exercise testing	
RER	1.11 (1.05-1.17)
Peak Watt	120 (105-150)
Peak heart rate	173 (164-184)
Peak predicted heart rate, %	94 (86-101)
Peak VO2, ml/kg/min	27.1 (22.4-30.0)
Peak predicted VO2, %	55 (47-65)

Values are reported as median (Q1-Q3) unless otherwise specified. TA; tricuspid atresia, HLHS; hypoplastic left heart syndrome, DILV; double inlet left ventricle, (cc)TGA; (congenital corrected) transposition of the great arteries, DORV; double outlet right ventricle, uAVSD; unbalanced atrioventricular septal defect, PA+IVS; pulmonary atresia with intact ventricular septum, RER; respiratory exchange ratio

Geometry and flow

Vessel CSA of the different segments of the TCPC are reported in Table 2. Absolute measured conduit CSA_{mean} was 100% (Q1-Q3 94-105), 95% (Q1-Q3 90-106) and 95% (Q1-Q3 72-105) of theoretical implanted conduit size in patients with 16,18 and 20mm conduits, respectively (p=0.42). The conduit CSA_{mean} normalized for conduit flow rate was significantly smaller compared to the normalized vessel CSA_{mean} of all other vessels (all P<0.001); a median 56,73 and 64% smaller compared to the subhepatic IVC, HVs and SVC, respectively, and 40 and 35% smaller compared to the LPA and RPA, respectively.

Table 2. Flow and geometry characteristics

	Flow (L/min)			Geometry		
	Average respiratory cycle	**Inspiration**	**Expiration**	**Absolute CSA_{mean} (mm^2)**	**Absolute CSA_{min} (mm^2)**	**Normalized CSA_{mean} (mm^2/L/min)**
Conduit	3.3 (2.5-4.0)	4.5 (3.7-5.3)	2.6 (1.9-3.3)	217 (199-249)	196 (182-230)	65 (54-90)
IVC	1.8 (1.5-2.2)	2.0 (1.6-2.4)	1.7 (1.3-2.1)	263 (222-303)	-	147 (122-170)
HVs	1.5 (1.0-1.8)	2.5 (1.8-3.0)	0.7 (0.5-1.2)	347 (303-405)	-	243 (183-352)
SVC	1.3 (1.0-1.6)	1.5 (1.2-1.8)	1.2 (1.0-1.5)	214 (192-262)	193 (165-224)	180 (133-216)
LPA	1.9 (1.3-2.3)	2.5 (1.7-2.9)	1.5 (1.1-1.9)	186 (150-236)	149 (109-192)	108 (89-153)
RPA (distal to RUL branch)	1.9 (1.5-2.3)	2.5 (2.0-2.8)	1.5 (1.1-1.8)	201 (167-231)	181 (134-215)	100 (84-136)

CSA; cross-sectional area, IVC/SVC; inferior/superior vena cava, RPA/LPA; right/left pulmonary artery, HV; hepatic veins, mm; millimeter, L/min; liter/minute

Total systemic venous return during the entire respiratory cycle was 4.5 (Q1-Q3 3.8-5.5) L/min in rest, increasing to 10.8 (Q1-Q3 8.4-12.5) L/min during simulated exercise. Flow rates during inspiration and expiration in the TCPC are reported in Table 2. Flow rates in all vessels were lowest during expiration and highest during inspiration (all P<0.001), most predominantly in the HVs (Table 2). Mean conduit flow during the entire respiratory cycle positively correlated with BSA, but considerable variability in flow rates was observed (Figure 1).

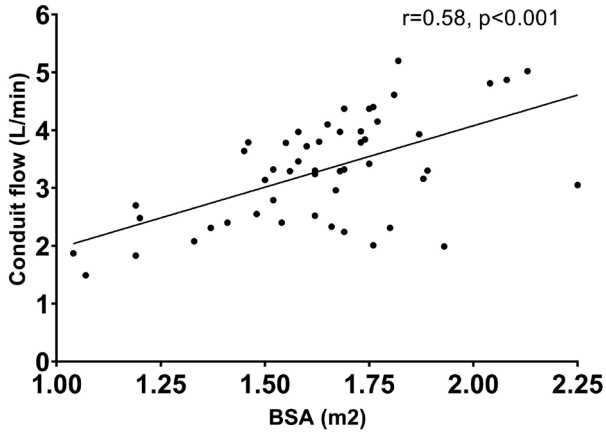

Figure 1. A moderate positive correlation is present between BSA and mean conduit flow rate along the entire respiratory cycle. The linear regression line is shown.

BSA; body surface area (Haycock).

Energetics

CFD derived energetics along the respiratory cycle are reported in Table 3, both for resting and simulated exercise conditions. No significant difference in energetics was present between gender.

Inspiration vs expiration

During rest, mean power loss was higher during inspiration (median 10.5mW, Q1-Q3 6.5-14.2) compared to expiration (3.7mW, Q1-Q3 2.5-6.3, p<0.001). Furthermore, the median pressure gradient was higher during inspiration (0.8mmHg, Q1-Q3 0.6-1.0) compared to expiration (0.5mmHg, Q1-Q3 0.4-0.7). No significant difference was present in normalized resistance between inspiration and expiration (Table 3).

Rest vs simulated exercise

Power loss, pressure gradient and normalized resistance all significantly increased from resting to simulated exercise conditions (all p<0.001, Table 3), most pronounced during inspiration for power loss and pressure gradient. From rest to exercise, the respiratory-cycle averaged power loss increased with a median factor of 6.9 (Q1-Q3 6.2-7.7), the pressure gradient increased with a factor of 3.0 (Q1-Q3 2.7-3.4) and the normalized resistance increased with a factor of 1.3 (Q1-Q3 1.2-1.5).

Table 3. Computational fluid dynamics results

	Resting conditions			Exercise conditions		
Energetics	**Average**	**Inspiration**	**Expiration**	**Average**	**Inspiration**	**Expiration**
Power loss, mW	6.8 (4.1-9.8)†,‡	10.5 (6.5-14.2)‡,§	3.7 (2.5-6.3)†,§	48.6 (27.4-70.5)†,‡	61.0 (33.5-86.3)‡,§	38.6 (19.0-57.6)†,§
Pressure gradient, mmHg	0.7 (0.5-0.8)†,‡	0.8 (0.6-1.0)‡,§	0.5 (0.4-0.7)†,§	2.0 (1.4-2.6)†,‡	2.3 (1.5-2.8)‡,§	1.8 (1.2-2.3)†,§
Normalized resistance, mmHg/L/min/m^2	0.23 (0.18-0.28)†,‡	0.21 (0.15-0.28)§	0.22 (0.18-0.27)§	0.29 (0.22-0.42)‡	0.29 (0.21-0.41)‡	0.29 (0.21-0.41)†,§
Thrombosis marker (n=15)	**Minimum (inspiration)**	**Maximum (expiration)**		**Minimum (inspiration)**	**Maximum (expiration)**	
Flow stagnation entire TCPC, %	1.2 (0.7-1.8)	6.2 (4.8-8.0)		0.4 (0.2-0.7)	1.5 (0.8-2.2)	
Flow stagnation conduit, %	0.0 (0.0-0.0)	0.5 (0.2-1.2)		0.0 (0.0-0.0)	0.0 (0.0-0.0)	

P-value <0.05 compared to inspiration†, expiration‡ or the entire respiratory cycle§. mW; miliwatt, mmHg; millimeter mercury, L/min; liter/minute

A moderate-strong inverse non-linear relationship was present between normalized conduit CSA_{mean} and power loss, pressure gradient and normalized resistance, both in rest and simulated exercise conditions (Figure 2). As derived from the regression curves in Figure 2B, a normalized conduit CSA_{mean} of ≤45mm^2/L/min corresponded to a median pressure gradient of ≥1.0 at rest and ≥3.0 during simulated exercise. A normalized conduit CSA_{mean} of ≥125mm^2/L/min corresponded to a pressure gradient of ≤1.0mmHg during both rest and simulated exercise. An example of streamline blood flow visualization and power loss heatmaps in two Fontan patients with a small and relatively large normalized conduit CSA_{mean} are illustrated in Figure 3. Pathline blood flow visualization during two respiratory cycles during resting and simulated exercise conditions are shown in Video 1&2.

Furthermore, a negative correlation was present between normalized conduit CSA_{mean} and the relative rest-to-exercise increase in power loss (ρ=-0.63, $p<0.001$), pressure gradient (ρ=-0.59, $p<0.001$) and normalized resistance (ρ=-0.50, $p<0.001$), indicating strongest increases in patients with smallest conduits.

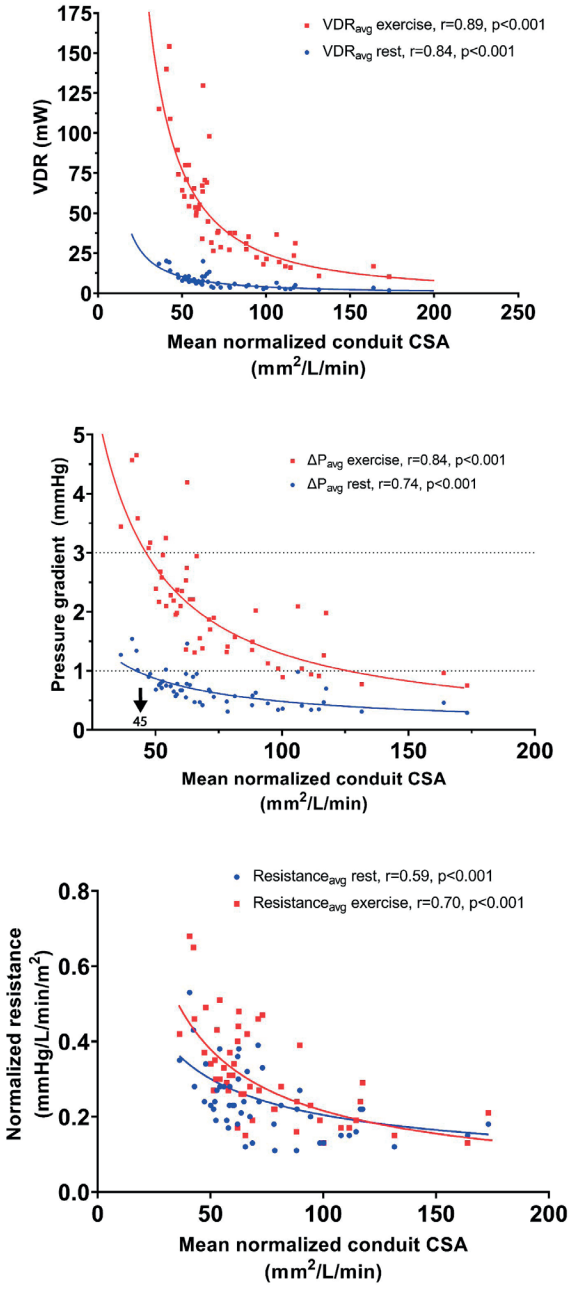

Figure 2. A moderate to strong inverse non-linear relationship is present between power loss (upper panel), pressure gradient (middle panel) and normalized resistance (lower panel) with normalized conduit cross sectional area, during both rest (blue) and simulated exercise (red). One significant outlier of normalized TCPC resistance was excluded from the analysis.

CSA; cross-sectional area, mW; milliwatt.

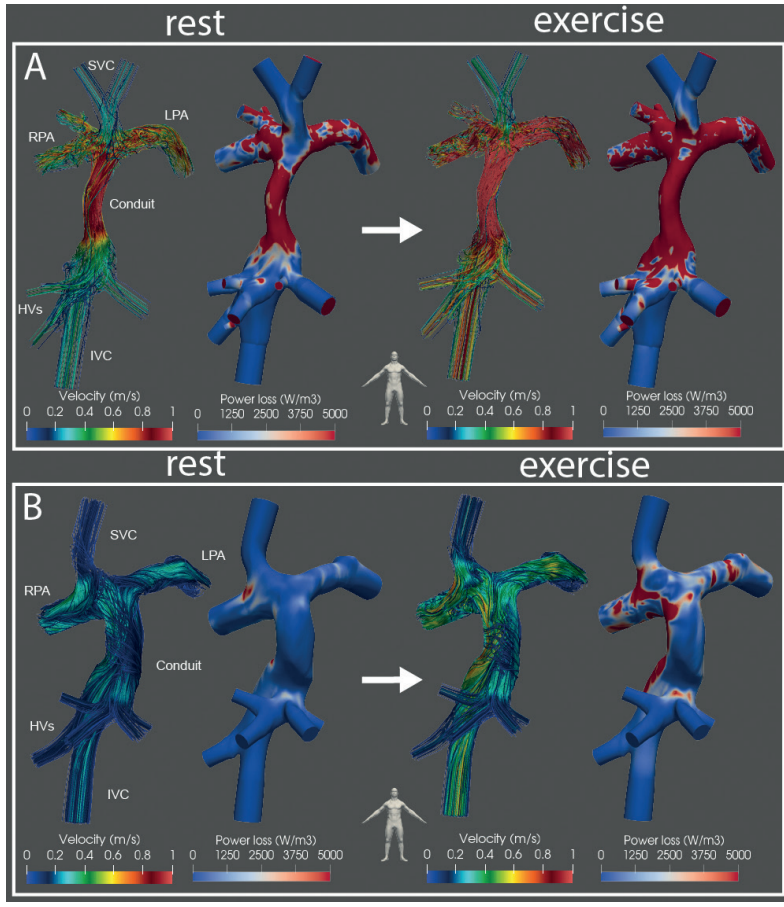

Figure 3. Velocity-colored streamline representation and power loss heatmaps of blood flow in the TCPC during peak inspiration is shown for 2 Fontan patients with a relatively small (A) and large (B) normalized conduit CSA_{mean}. Note the strong increase in blood flow velocity and power loss at the junction between the IVC/HVs and the extracardiac conduit extending into the PAs in patient A, indicating the presence of an functionally undersized conduit.

Patient A. 16yr, BSA 1.82m^2, 16mm implanted conduit, mean conduit flow respiratory cycle 5.2 L/min, normalized conduit CSA_{mean} 36mm^2/L/min. CFD energetics (rest/exercise): Power loss 18.3/115.1mW, pressure drop 1.3/3.4mmHg, normalized resistance 0.35/0.41 mmHg/L/min/m^2.

Patient B. 16yr, BSA 1.76m^2, 18mm implanted conduit, mean conduit flow respiratory cycle 2.0 L/min, normalized conduit CSA_{mean} 173mm^2/L/min. CFD energetics (rest/exercise): Power loss 1.7/10.3mW, pressure drop 0.3/0.8mmHg, normalized resistance 0.18/0.21 mmHg/L/min/m^2.

A weak negative correlation was present between normalized resistance of the TCPC and peak VO2 during both rest (r=-0.41, p=0.009) and during simulated exercise (r=-0.37, p=0.020). Normalized resistance correlated with predicted peak VO2 during rest (r=-0.36, p=0.024) and during simulated exercise (r=-0.37, p=0.020, Figure 4). No

correlation was found between power loss or pressure gradient and peak VO2 (r=-0.25, p=0.10 for both power loss and pressure gradient).

Flow stagnation volume

Maximal flow stagnation volume (expiration) in rest in the entire TCPC was 6.2% (Q1-Q3 4.8-8.0) of the total volume. Minimal flow stagnation (inspiration) was significantly smaller (median 1.2%, Q1-Q3 0.7-1.8, p<0.001) due to the increase in flow during inspiration (Table 3). Increased flow during simulated exercise further reduced maximal (median 1.5%, Q1-Q3 0.8-2.2) and minimal (median 0.4%, Q1-Q3 0.2-0.7) flow stagnation volume. Both minimal and maximal flow stagnation volume in the conduit only were absent/negligible (Table 3). No significant differences in flow stagnation volume in the conduit were found between patients with implanted 16,18 and 20mm conduit sizes.

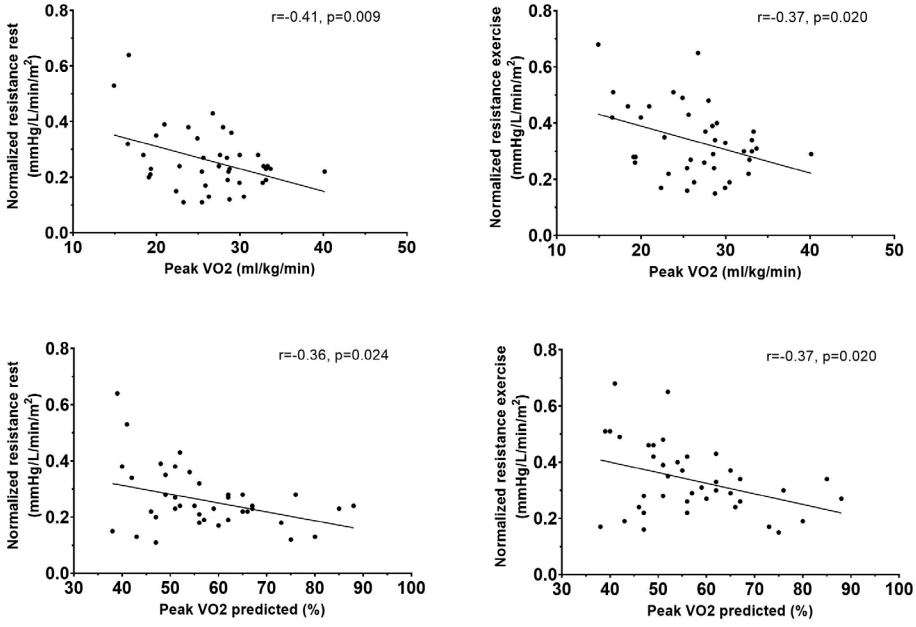

Figure 4. A weak inverse linear correlation is observed between normalized resistance of the TCPC and peak VO2 (upper panels) and predicted peak VO2 (lower panels) in rest (left panels) and during simulated exercise (right panels).

Discussion

This study shows that extracardiac conduits of 16 to 20mm have become undersized for teenage and adolescent Fontan patients on average 13 years after Fontan completion. Main results are a significantly smaller normalized conduit CSA_{mean} compared to the other TCPC vessels. Furthermore, pressure gradients and resistance in the TCPC increased non-linearly with decreasing normalized conduit CSA. Finally, a weak correlation was observed between TCPC resistance and peak VO2. Especially patients with a normalized conduit CSA_{mean} ≤45mm^2/L/min showed important pressure gradients in the TCPC, most pronounced during simulated exercise, and may require close monitoring for Fontan failure. In patients with a univentricular heart defect, the Fontan procedure is the palliative treatment of choice. The current recommendation is to implant a slightly oversized (16 to 20mm extracardiac Goretex conduit) in children at the age of 2-4 years, thereby aiming to avoid somatic overgrowth necessitating reintervention.(1,17) However, optimal conduit size for adult Fontan patients remains elusive mainly because no clear definition is present to describe conduit adequacy. Recently, our group observed important velocity accelerations from the subhepatic IVC towards the conduit indicating that these conduits have become too small.(6,18) The current study adds important information by assessment of the functional conduit size to describe conduit adequacy: conduit CSA_{mean} normalized for conduit flow rate, and by characterizing the hemodynamic performance of the TCPC using CFD at rest and during simulated exercise. Of note, in the absence of a distinct conduit stenosis, functional conduit size can be easily obtained from a 2D flow measurement at the level of the conduit which is part of standard Fontan MRI protocols.

Conduit adequacy

In our cohort of on average 16 year old patients with a median conduit flow rate of 3.3 L/min, a median normalized conduit CSA of 65 mm^2/L/min was present, significantly smaller compared to the other vessels in the TCPC. For comparison, Itatani et al. recommended the use of 16-18mm conduits (conduit CSA of 201-254mm^2) for Fontan completion using CFD models based on 36 months old children with an average conduit flow rate of approximately 0.85 L/min in rest.(16) This would correspond to a normalized conduit CSA_{mean} of approximately 240-300 mm^2/L/min. In addition, flow stagnation was absent or negligible in both the entire TCPC and in the conduit only in our cohort, further emphasizing that blood flow stasis caused by oversizing is not a relevant problem anymore in 16-20mm conduits when reaching the adolescent age. However, other factors associated with thrombus formation such as high shear flows may become increased by undersized conduits and is subject to future research.(19)

To assess the hemodynamic consequence of the reduced normalized conduit CSA_{mean}, we used CFD modelling in rest and during simulated exercise for the quantification

of the power loss based pressure gradient and resistance of the TCPC.(10) The ability to simulate blood flow during exercise is one great advantage of CFD compared to conventional diagnostics such as catheterization, which is usually only limited to resting conditions.(20) Main results of the CFD analysis showed a strong inverse non-linear correlation between normalized conduit CSA_{mean} and pressure gradients, reaching ≥1mmHg in rest and ≥3mmHg during simulated exercise in patients with a conduit ≤45mm^2/L/min. Especially during inspiration in exercise, pressure gradients in the order of 5mmHg were observed in patients with smallest functional conduit sizes. Additionally, patients with smallest functional conduit sizes showed a higher increase in energetics from rest-to-exercise than patients with larger functional conduits. Importantly, the use of CFD simulated exercise showed that in patients with a conduit CSA of 45-125mm^2/L/min, pressure gradients were relatively low (<1mmHg) in rest, but significantly increased during simulated exercise to values of 1-3mmHg which may be of clinical significance. This data therefore emphasizes the current drawbacks of evaluating TCPC hemodynamics using catheterization in rest, as small pressure gradients in rest may mask important pressure gradients during exercise.(21)

Currently, no cut-off values for clinically relevant pressure gradients in the TCPC are defined that may indicate the need for intervention, but catheterization derived pressure gradients as low as 1mmHg may already be an indication of clinically relevant Fontan pathway obstruction.(22) Our data indicate that patients with a conduit ≤45mm^2/L/min may require close monitoring, as further decline in functional conduit size is expected to lead to a non-linear increase in pressure gradient and resistance. A recent study showed that dilatation of the conduit significantly improved hemodynamics, but will depend on the increase in conduit CSA that can be accomplished.(23) On the other hand, pressure gradients in the TCPC were relatively small in the majority of patients and the expected reduction in pressure gradients associated with conduit replacement may be insufficient to justify the risk of reoperation. It should also be noted that our study cohort represented patients in overall good clinical condition without any signs of Fontan failure. However, the chronic adverse effects of decreasing flow efficiency and subsequent elevation in CVP and/or gradual decrease in preload may take more time to become clinically apparent.

Relevance for surgical strategy

The results of our study raise concern that the current surgical strategy may lead to suboptimal hemodynamics of the Fontan circulation for both young children and adolescent Fontan patients. In young children, oversizing increases thrombosis risk and also lead to increased energy losses(16,24,25), while in adolescent Fontan patients these conduits become undersized. Favorable hemodynamics (pressure gradient <1mmHg during both rest and exercise) were observed in patients with a conduit CSA

of ≥125mm^2/L/min. This corresponds to conduit sizes of between 375mm^2 (i.e. ±22mm) and 625mm^2 (±28mm) for patients with 3-5L/min conduit flow. These values would be in line with suprahepatic IVC diameters observed in healthy persons(26), and with Fontan tunnel CSA (420-580mm^2, i.e. 23-27mm) observed in 10-15 year old Fontan patients with a lateral tunnel.(6,27,28) However, implanting larger conduit sizes at the initial Fontan operation is not feasible due to anatomical constraints and the increased risk of conduit thrombosis.(16,24) Based on our observations, in our opinion alternative surgical strategies should be explored such as implanting other, non-rigid materials to optimize future hemodynamics, including dilatable ePTFE grafts (PECA labs) and stress the need for tissue-engineered grafts with growth potential.(29)

Limitations

Flow rates were modelled with respect to the respiratory cycle, ignoring the effect of the cardiac cycle on flow rates. However, since flow pulsatility is almost entirely related to the respiratory cycle(30,31), inaccuracies are likely small. No patient-specific exercise flow data was available necessitating the use of adapted cohort averaged increases in flow from rest to exercise. However, a previous study found an increase in CVP from 9 towards 20mmHg during lower leg exercise and TCPC pressure gradients of 3-5mmHg found in our study in patients with smallest conduits are in line with the rise seen in CVP from rest to exercise.(32) The measured conduit CSA_{mean} exceeded the theoretical conduit CSA in some patients and this overestimation is most likely related to the resolution of the MRI acquisitions. Lastly, the potential improvement in TCPC hemodynamics with larger conduits was not studied and could only be indirectly determined from the curves in Figure 2. CFD models using virtual surgery could be useful to validate the improvement in TCPC hemodynamics with implantation of larger conduit sizes.

Conclusions

Extracardiac conduits of 16 to 20mm have become relatively undersized in teenage and adolescent Fontan patients. Pressure gradients and resistance in the TCPC increased non-linearly with decreasing normalized conduit CSA and a weak correlation was observed between normalized TCPC resistance and peak VO2. Patients with a conduit ≤45mm^2/L/min showed important pressure gradients in the TCPC, most predominantly during simulated exercise, and may require close monitoring for worsening of Fontan pathway obstruction. Furthermore, these observations question the long-term efficacy of the current surgical Fontan approach using 16-20 mm conduits and alternative surgical strategies should be explored to optimize future hemodynamics in adult Fontan patients.

References

1. Rychik J, Atz AM, Celermajer DS et al. Evaluation and Management of the Child and Adult With Fontan Circulation: A Scientific Statement From the American Heart Association. Circulation 2019.
2. Gewillig M, Brown SC. The Fontan circulation after 45 years: update in physiology. Heart 2016;102:1081-6.
3. Rijnberg FM, Hazekamp MG, Wentzel JJ et al. Energetics of Blood Flow in Cardiovascular Disease: Concept and Clinical Implications of Adverse Energetics in Patients With a Fontan Circulation. Circulation 2018;137:2393-2407.
4. Sundareswaran KS, Pekkan K, Dasi LP et al. The total cavopulmonary connection resistance: a significant impact on single ventricle hemodynamics at rest and exercise. Am J Physiol Heart Circ Physiol 2008;295:H2427-35.
5. Tang E, Restrepo M, Haggerty CM et al. Geometric characterization of patient-specific total cavopulmonary connections and its relationship to hemodynamics. JACC Cardiovasc Imaging 2014;7:215-24.
6. Rijnberg FM, van der Woude SFS, Hazekamp MG et al. Extracardiac conduit adequacy along the respiratory cycle in adolescent Fontan patients. European Journal of Cardio-Thoracic Surgery 2021.
7. Yushkevich PA, Gerig G. ITK-SNAP: An Intractive Medical Image Segmentation Tool to Meet the Need for Expert-Guided Segmentation of Complex Medical Images. IEEE Pulse 2017;8:54-57.
8. Antiga L, Piccinelli M, Botti L, Ene-Iordache B, Remuzzi A, Steinman DA. An image-based modeling framework for patient-specific computational hemodynamics. Med Biol Eng Comput 2008;46:1097-112.
9. Rijnberg FM, Juffermans JF, Hazekamp MG et al. Segmental assessment of blood flow efficiency in the total cavopulmonary connection using 4D flow MRI: vortical flow is associated with increased viscous energy loss. European Heart Journal Open 2021.
10. Haggerty CM, Restrepo M, Tang E et al. Fontan hemodynamics from 100 patient-specific cardiac magnetic resonance studies: a computational fluid dynamics analysis. J Thorac Cardiovasc Surg 2014;148:1481-9.
11. Wei Z, Singh-Gryzbon S, Trusty PM et al. Non-Newtonian Effects on Patient-Specific Modeling of Fontan Hemodynamics. Ann Biomed Eng 2020;48:2204-2217.
12. Wei Z, Whitehead KK, Khiabani RH et al. Respiratory Effects on Fontan Circulation During Rest and Exercise Using Real-Time Cardiac Magnetic Resonance Imaging. Ann Thorac Surg 2016;101:1818-25.
13. Hjortdal VE, Emmertsen K, Stenbog E et al. Effects of exercise and respiration on blood flow in total cavopulmonary connection: a real-time magnetic resonance flow study. Circulation 2003;108:1227-31.
14. Khiabani RH, Whitehead KK, Han D et al. Exercise capacity in single-ventricle patients after Fontan correlates with haemodynamic energy loss in TCPC. Heart 2015;101:139-43.
15. Wei ZA, Tree M, Trusty PM, Wu W, Singh-Gryzbon S, Yoganathan A. The Advantages of Viscous Dissipation Rate over Simplified Power Loss as a Fontan Hemodynamic Metric. Ann Biomed Eng 2018;46:404-416.
16. Itatani K, Miyaji K, Tomoyasu T et al. Optimal conduit size of the extracardiac Fontan operation based on energy loss and flow stagnation. Ann Thorac Surg 2009;88:565-72; discussion 572-3.

17. Daley M, d'Udekem Y. The optimal Fontan operation: Lateral tunnel or extracardiac conduit? J Thorac Cardiovasc Surg 2020.
18. Rijnberg FM, van Assen HC, Hazekamp MG, Roest AAW, Westenberg JJM. Hemodynamic Consequences of an Undersized Extracardiac Conduit in an Adult Fontan Patient Revealed by 4-Dimensional Flow Magnetic Resonance Imaging. Circ Cardiovasc Imaging 2021;14:e012612.
19. van Rooij BJM, Zavodszky G, Azizi Tarksalooyeh VW, Hoekstra AG. Identifying the start of a platelet aggregate by the shear rate and the cell-depleted layer. J R Soc Interface 2019;16:20190148.
20. Whitehead KK, Pekkan K, Kitajima HD, Paridon SM, Yoganathan AP, Fogel MA. Nonlinear power loss during exercise in single-ventricle patients after the Fontan: insights from computational fluid dynamics. Circulation 2007;116:I165-71.
21. Shachar GB, Fuhrman BP, Wang Y, Lucas RV, Lock JE. Rest and exercise hemodynamics after the Fontan procedure. Circulation 1982;65:1043-1048.
22. Alsaied T, Rathod RH, Aboulhosn JA et al. Reaching consensus for unified medical language in Fontan care. ESC Heart Fail 2021.
23. Hagler DJ, Miranda WR, Haggerty BJ et al. Fate of the Fontan connection: Mechanisms of stenosis and management. Congenit Heart Dis 2019;14:571-581.
24. Alexi-Meskishvili V, Ovroutski S, Ewert P et al. Optimal conduit size for extracardiac Fontan operation. Eur J Cardiothorac Surg 2000;18:690-5.
25. Ascuitto RJ, Kydon DW, Ross-Ascuitto NT. Pressure loss from flow energy dissipation: relevance to Fontan-type modifications. Pediatr Cardiol 2001;22:110-5.
26. Ettinger E. Angiocardiographic measurement of the cardiac segment of the inferior vena cava in health and in cardiovascular disease. Circulation 1962;26:508-15.
27. Bossers SS, Cibis M, Gijsen FJ et al. Computational fluid dynamics in Fontan patients to evaluate power loss during simulated exercise. Heart 2014;100:696-701.
28. Restrepo M, Mirabella L, Tang E et al. Fontan pathway growth: a quantitative evaluation of lateral tunnel and extracardiac cavopulmonary connections using serial cardiac magnetic resonance. Ann Thorac Surg 2014;97:916-22.
29. Szafron JM, Ramachandra AB, Breuer CK, Marsden AL, Humphrey JD. Optimization of Tissue-Engineered Vascular Graft Design Using Computational Modeling. Tissue Eng Part C Methods 2019;25:561-570.
30. Gabbert DD, Hart C, Jerosch-Herold M et al. Heart beat but not respiration is the main driving force of the systemic venous return in the Fontan circulation. Sci Rep 2019;9:2034.
31. van der Woude SFS, Rijnberg FM, Hazekamp MG et al. The Influence of Respiration on Blood Flow in the Fontan Circulation: Insights for Imaging-Based Clinical Evaluation of the Total Cavopulmonary Connection. Front Cardiovasc Med 2021;8:683849.
32. Van De Bruaene A, La Gerche A, Claessen G et al. Sildenafil improves exercise hemodynamics in Fontan patients. Circ Cardiovasc Imaging 2014;7:265-73.

Supplementary materials

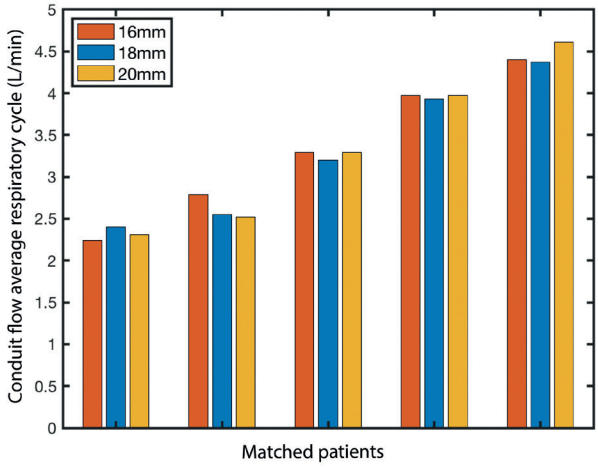

Supplemental Figure 1. Fifteen patients with 16,18 and 20mm conduits were matched based on average conduit flow rate along the respiratory cycle.

Supplemental table 1. MRI details of TCPC anatomic and velocity acquisitions

MRI details	2D transversal and sagittal stacks	2D realtime PC-MRI
Slice thickness (mm)	5, 2.5 overlap	6
Acquired in-plane spatial resolution (mm)	1.8x1.7	2.5 x 2.5
Reconstructed in-plane spatial resolution (mm)	0.9 x 0.9 mm	1.1 x 1.1
Acquired temporal resolution (ms)	-	63-67ms
Nr of samples	-	250
Respiratory compensation	navigator	-
Acceleration methods	SENSE factor 1.5	SENSE factor 3, EPI 11

All MRI examinations were performed on a 3T Philips MRI scanner (Ingenia, Philips Healthcare, Best, the Netherlands). mm; millimetre, PC-MRI; phase contrast magnetic resonance imaging, EPI; echo planar imaging